Dimensionless parameter predicts bacterial prodrug success

Brandon Alexander Holt[1] (iD), McKenzie Tuttle[1], Yilin Xu[1], Melanie Su[1], Joachim J Røise[2] (iD), Xioajian Wang[3] (iD), Niren Murthy[2] & Gabriel A Kwong[1,4,5,6,7,8,9,*] (iD)

Abstract

Understanding mechanisms of antibiotic failure is foundational to combating the growing threat of multidrug-resistant bacteria. Prodrugs—which are converted into a pharmacologically active compound after administration—represent a growing class of therapeutics for treating bacterial infections but are understudied in the context of antibiotic failure. We hypothesize that strategies that rely on pathogen-specific pathways for prodrug conversion are susceptible to competing rates of prodrug activation and bacterial replication, which could lead to treatment escape and failure. Here, we construct a mathematical model of prodrug kinetics to predict rate-dependent conditions under which bacteria escape prodrug treatment. From this model, we derive a dimensionless parameter we call the Bacterial Advantage Heuristic (*BAH*) that predicts the transition between prodrug escape and successful treatment across a range of time scales (1–10^4 h), bacterial carrying capacities (5×10^4–10^5 CFU/μl), and Michaelis constants ($K_M = 0.747$–7.47 mM). To verify these predictions *in vitro*, we use two models of bacteria-prodrug competition: (i) an antimicrobial peptide hairpin that is enzymatically activated by bacterial surface proteases and (ii) a thiomaltose-conjugated trimethoprim that is internalized by bacterial maltodextrin transporters and hydrolyzed by free thiols. We observe that prodrug failure occurs at *BAH* values above the same critical threshold predicted by the model. Furthermore, we demonstrate two examples of how failing prodrugs can be rescued by decreasing the *BAH* below the critical threshold via (i) substrate design and (ii) nutrient control. We envision such dimensionless parameters serving as supportive pharmacokinetic quantities that guide the design and administration of prodrug therapeutics.

Keywords antibiotic failure; bacteria; enzymes; minimum inhibitory concentration; prodrugs

Introduction

The rise of multidrug-resistant bacteria coupled with the lack of newly developed antibiotic treatment strategies has created a serious public health threat (Baquero *et al*, 2008; Gullberg *et al*, 2011). Antibiotic success is markedly improved by proper titration of drugs, as overdosing leads to off-target toxicity and underdosing increases the likelihood of pathogens developing resistance (Opatowski *et al*, 2010). However, optimal drug doses are difficult to achieve over the course of treatment because infection burden changes dynamically over time, creating a moving target (Opatowski *et al*, 2010; Iizumi *et al*, 2017). Prodrugs, which represent ~10% of all FDA-approved drugs in the last decade (Rautio *et al*, 2018a), are a promising solution because they present multiple strategies for reviving existing or previously discarded antibiotics (Jubeh *et al*, 2020); these strategies include increasing bioavailability and solubility, reducing off-target effects, or targeting bacteria-specific enzymes. For example, a prodrug of ciprofloxacin was developed that reduced off-target toxicity while selectively targeting bacteria expressing ß-lactamase (i.e., a resistance enzyme that degrades ß-lactam antibiotics) (Evans *et al*, 2019). Prodrug forms of Triclosan (Howse *et al*, 2019), Carvacrol (Marinelli *et al*, 2019), and multiple nucleoside derivatives (Negrya *et al*, 2020) were developed which increased solubility while maintaining antimicrobial efficacy. In this work we focus specifically on antibiotic prodrugs, a subset of prodrugs that includes compounds such as ganciclovir (Al-Badr & Ajarim, 2018) and isoniazid (Metcalfe *et al*, 2008), which are

1 Wallace H. Coulter Department of Biomedical Engineering, Georgia Tech College of Engineering and Emory School of Medicine, Atlanta, GA, USA
2 Department of Bioengineering, Innovative Genomics Institute, University of California, Berkeley, CA, USA
3 Institute of Advanced Synthesis, School of Chemistry and Molecular Engineering, Nanjing Tech University, Nanjing, China
4 Parker H. Petit Institute of Bioengineering and Bioscience, Atlanta, GA, USA
5 Institute for Electronics and Nanotechnology, Georgia Tech, Atlanta, GA, USA
6 Integrated Cancer Research Center, Georgia Tech, Atlanta, GA, USA
7 Georgia ImmunoEngineering Consortium, Georgia Tech and Emory University, Atlanta, GA, USA
8 Emory School of Medicine, Atlanta, GA, USA
9 Emory Winship Cancer Institute, Atlanta, GA, USA
   *Corresponding author. Tel: +1 404 385 3746; E-mail: gkwong@gatech.edu

administered as biologically inactive forms and are enzymatically activated into their parent form by the pathogen.

Despite their growing importance, prodrugs are critically understudied in the context of potential failure mechanisms that may arise during treatment. Currently, failure mechanisms fall into three distinct categories—resistance, persistence, and tolerance—which are characterized by the change in drug concentration and exposure time required to kill bacteria. For example, resistance is characterized by genetic mutations or phenotypic changes which result in bacteria requiring significantly higher concentrations of antibiotic (minimum inhibitory concentration, MIC) to be lethal. In contrast, bacteria exhibiting tolerance or persistence require increased drug exposure time (minimum duration for killing, MDK) (Brauner *et al*, 2016). However, prodrug activation introduces an additional reaction step; this two-step (Jain *et al*, 2009) mechanism (i.e., activation + killing) creates variability in the concentration and duration required for killing, which suggests that classification metrics such as MIC and MDK may not map directly from parent to prodrugs. Computational studies have shown that the prodrug activation step results in distinct differences in kinetics between parent and prodrug forms of the same compound (Jackson *et al*, 2000; Murphy *et al*, 2011; Cho & Yoon, 2018). For example, agent-based simulations revealed that the rate of prodrug activation (i.e., catalytic efficiency, k_{cat}/K_M) had a strong effect on the MIC of each compound (Murphy *et al*, 2011). Furthermore, empirical studies have found there to be differences in MIC between parent and prodrug forms, as well as higher variance in prodrug MIC across bacterial strains, relative to the parent drug (Wang *et al*, 2018; Evans *et al*, 2019; Yang *et al*, 2021).

Here, we develop a mathematical model of bacteria-prodrug systems to probe failure mechanisms and identify a prodrug-specific metric distinct from MIC to classify failure. We apply our model to two *in vitro* systems: (i) a prodrug of a cationic antimicrobial peptide (AMP) polyarginine (R9) targeting DH5α *E. coli* and (ii) a prodrug of trimethoprim (TMP) targeting UTI89 *E. coli*. The polyarginine AMP is formulated as a prodrug by charge complexation with anionic peptides connected by a modular protease-cleavable linker substrate (Olson *et al*, 2009, 2010; Forde *et al*, 2014). We design the linker substrate to be cleaved by *E. coli* protease OmpT, such that increasing concentrations of bacteria activate higher concentrations of free AMP. The trimethoprim prodrug comprises thiomaltose conjugated to trimethoprim via a self-immolative disulfide linker, which releases TMP-OH upon cleavage by free thiols inside bacterial cells without affecting the toxicity of the drug (Wang *et al*, 2018). Free TMP-OH then kills bacteria by inhibiting tetrahydrofolic acid synthesis, which is a necessary cofactor for thymidine, purine, and bacterial DNA synthesis (Masters *et al*, 2003).

In both prodrug systems, we observe experimental conditions where (i) bacteria proliferate in the presence of active drug by consistently outpacing prodrug activation at all stages of growth (i.e., log phase, stationary phase) as well as (ii) conditions where bacteria are successfully treated. To create a metric that predicts the transition between these treatment outcomes we identify a dimensionless parameter, the Bacterial Advantage Heuristic (*BAH*). Dimensionless parameters characterize physical systems across a wide range of scales (e.g., time, length, temperature, etc.); for example, the dimensionless Reynolds number (*Re*) predicts the transition from laminar (low *Re*) to turbulent (high *Re*) fluid flow (Batchelor, 2000).

Similarly, we show that the *BAH* predicts the transition from successful treatment (low *BAH*) to prodrug escape (high *BAH*) with high accuracy (AUROC = 1.00, $n = 9$) across a range of environmental conditions (e.g., temperatures, nutrient levels). We envision that such a dimensionless parameter may be useful for predicting prodrug success across a broad range of treatment conditions which may extend to clinical use cases. These quantitative insights may inform future drug design and treatment protocols for improving the impact of prodrugs in combatting antibiotic resistance.

Results

A computational model of bacteria-prodrug activation kinetics

Models of parent drug kinetics (Nielsen *et al*, 2007, 2011; Nguyen *et al*, 2014) generally do not have feedback loops, meaning the drug population affects the bacterial population (i.e., bacterial death, green arrow), but the bacteria do not influence the drug population (Fig 1A). By comparison, models of prodrug kinetics do have a feedback loop as bacteria determine the growth of the drug population (i.e., activation, green arrow), which kills bacteria. We hypothesized that this feedback loop creates competition between the rate of prodrug activation and the rate of bacterial death (Fig 1B). Interestingly, this may enable possibilities where bacteria escape prodrug treatment; for example, when the activation rate is decreased to a near-zero value (i.e., activation, red arrow with "X"), then the rate of bacterial death is minimized, allowing the bacteria population to grow uncontrolled (Fig 1C). To quantitatively understand the rate-competition between bacteria and prodrugs, we built a mathematical compartment model using a system of nonlinear ordinary differential equations (ODE). In this system, the three dynamic populations were the Bacteria, B, the Locked drug (i.e., prodrug), L, and the Unlocked drug (i.e., parent drug), U, for which we formulated governing ODEs by considering the system parameters that affect population change over time. We modeled the bacteria population, B, as increasing the rate of prodrug conversion (i.e., L to U) and the unlocked drug population U as increasing the rate of bacterial death (Fig 1B). To account for the fact that bacterial growth rate, r, slows down as environmental resources become limiting (i.e., carrying capacity, B_{max}), we used a logistic growth model (Fujikawa *et al*, 2003), which produces an S-shaped curve and has been used extensively in biology to study population expansion (Verhulst, 1845) and tumor growth (Atuegwu *et al*, 2013). In contrast, we model the rate of bacterial death as proportional to the concentration of unlocked drug, U, and the concentration of Bacteria, B, according to a proportionality rate constant, a, which represents the bacterial death rate constant (Equation 1.1, Table EV2).

$$\frac{dB}{dt} = rB\left(1 - \frac{B}{B_{\max}}\right) - aBU \qquad (1.1)$$

To model the rate of activation of locked drugs, L, we applied Michaelis–Menten (MM) kinetics (Menten & Michaelis, 1913), where the rate of substrate activation is determined by the catalytic rate of the reaction, k_{cat}, and the half-maximal substrate concentration, K_M. Here, we modeled the locked drug as the substrate and the unlocked drug as the product; therefore, we modeled the bacteria as
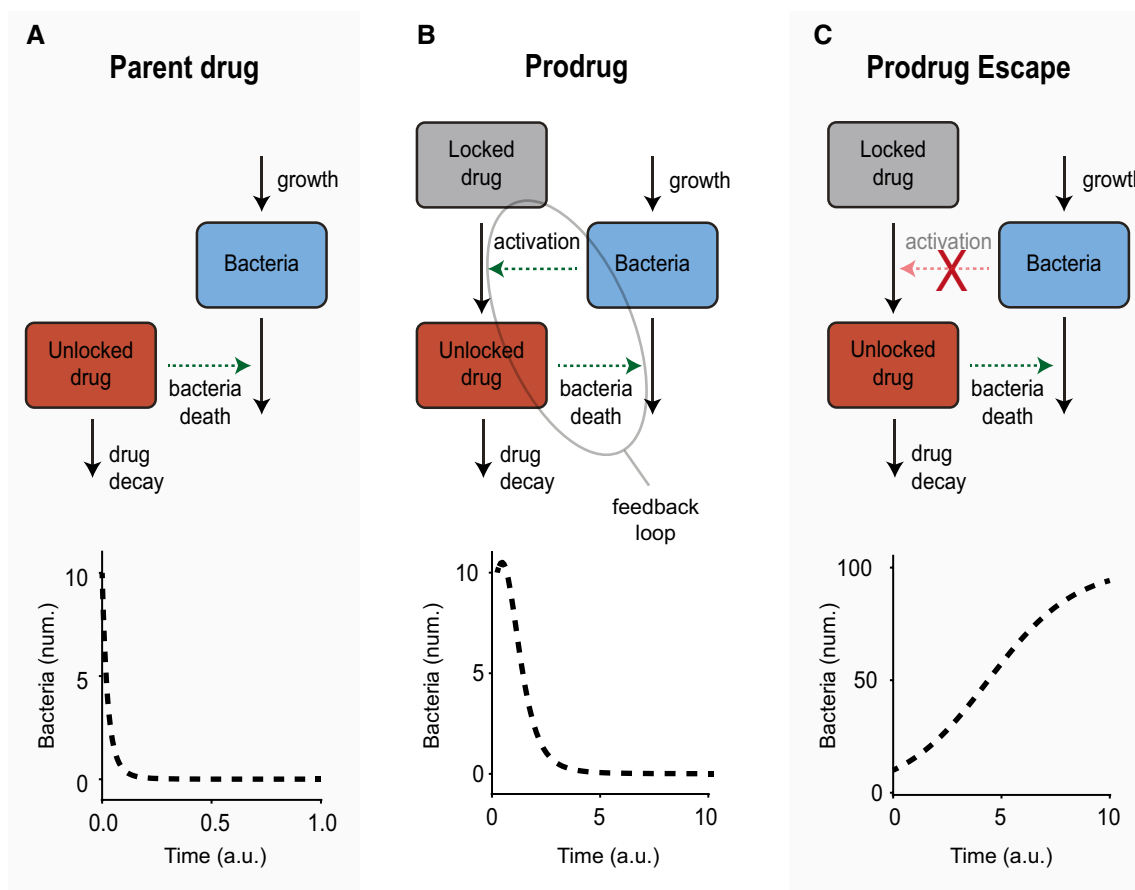
Figure 1. A computational model of bacteria-prodrug activation kinetics.

A Standard model of bacteria-drug kinetics (i.e., the parent drug model). (Top) General mass action schematic of bacteria population (blue box) versus the unlocked drug population (red box). The unlocked drug increases the rate of bacterial death (i.e., green arrow labeled "bacteria death"). (Bottom) Computational results of the parent drug model, plotting the living bacteria population over time.

B Our model of bacteria-prodrug kinetics (i.e., the prodrug model). (Top) General mass action schematic of the locked drug (gray box), which is activated (green arrow labeled "activation") by the bacteria (blue box) and converted into the unlocked drug (red box). (Bottom) Computational results of the prodrug model, plotting the decay in the living bacteria population over time.

C The model of prodrug escape, (Top) where the activation rate of the locked drug is lowered significantly (red arrow with "X"). (Bottom) Computational results of the prodrug escape model, plotting the growth in the number of living bacteria over time. In all plots, bacteria are plotted as number of cells (num., y-axis), and time is plotted in arbitrary units (a.u., x-axis).

the enzymatic population because the bacteria convert locked drug (i.e., substrate) to unlocked drug (i.e., product) (Equation 1.2). To apply MM kinetics, we assumed our system constituted a well-mixed solution of freely diffusing substrates (i.e., locked drug) in large excess relative to the number of bacteria enzymes, which were valid assumptions for our downstream studies since prodrugs were present at concentrations ~10^2 micromolar in an aqueous environment relative to a maximum bacterial concentration of ~10^{-6} micromolar. Because the total amount of drug is conserved, we defined the MM activation rate of unlocked drug, U, as opposite of the degradation rate of locked drug L. We further included a term to account for the loss of unlocked drug according to a proportionality constant, b, which represents the drug decay rate constant (Equation 1.3, Table EV2).

$$\frac{dL}{dt} = -k_{cat}B\frac{L}{K_m + L} \quad (1.2)$$

$$\frac{dU}{dt} = k_{cat}B\frac{L}{K_m + L} - bBU \quad (1.3)$$

We performed a linear stability analysis on this system of differential equations and found that there are two unique steady-state solutions. The analysis revealed that the solution that includes the result $B_{s.s} = B_{max}$ is stable, whereas the other solution (i.e., $B_{s.s} = 0$) is unstable (Supplementary analysis).

Predicting prodrug success with a dimensionless parameter

We hypothesized that the primary mechanism controlling prodrug success or escape is tied to the competition between bacterial growth and prodrug activation (Fig 1B and C). Therefore, we chose to focus our studies on a dimensionless parameter that represents the competing ratio of growth rate (r) divided by prodrug activation rate (k_{cat}). We defined this dimensionless parameter as the Bacterial

Advantage Heuristic (*BAH*) and we calculated the log of this quantity since bacterial quantities span across several orders of magnitude (Equation 2.1).

$$BAH = \log_{10}\left(\frac{r}{k_{cat}}\right) \qquad (2.1)$$

In this form, the *BAH* is larger when the rate of bacterial growth (r) increases relative to the rate of prodrug activation (k_{cat}); according to our hypothesis, conditions with larger *BAH* values would yield an increased probability of prodrug escape. To verify this computationally, we sought to determine the critical *BAH* value (BAH_{crit}) that distinguishes prodrug escape from prodrug success (Fig 2A). Using our mathematical model, we simulated > 2,500 prodrug treatment conditions covering a range of values for r

(3×10^{-2}–10^0 h^{-1}), B_{max} (5×10^4–10^5 CFU/µl), k_{cat} (2.5×10^9–10^{11} h^{-1}), and K_m (0.747–7.47 mM) each spanning at least an order of magnitude (Fig 2B). We fixed the bacteria death rate constant, a, and the drug decay rate constant, b, because these parameters are closely linked to the identity of the bacterial strain and prodrug formulation, meaning that changing these values would reflect an entirely different treatment scenario altogether (i.e., different bacteria species and/or drug). We plotted the number of surviving bacteria at various time points divided by the bacterial carrying capacity of the system to normalize against different B_{max} values. We observed that at early time points (i.e., $t < 24$ h) conditions with smaller *BAH* certainly reached a final value of 0, whereas conditions with larger *BAH* resulted in a distribution between 0 and 1 (Fig 2C–E). However, the model showed that as the system moves toward steady-state (i.e., $t > 24$ h), conditions with high *BAH* approach a final value of 1,
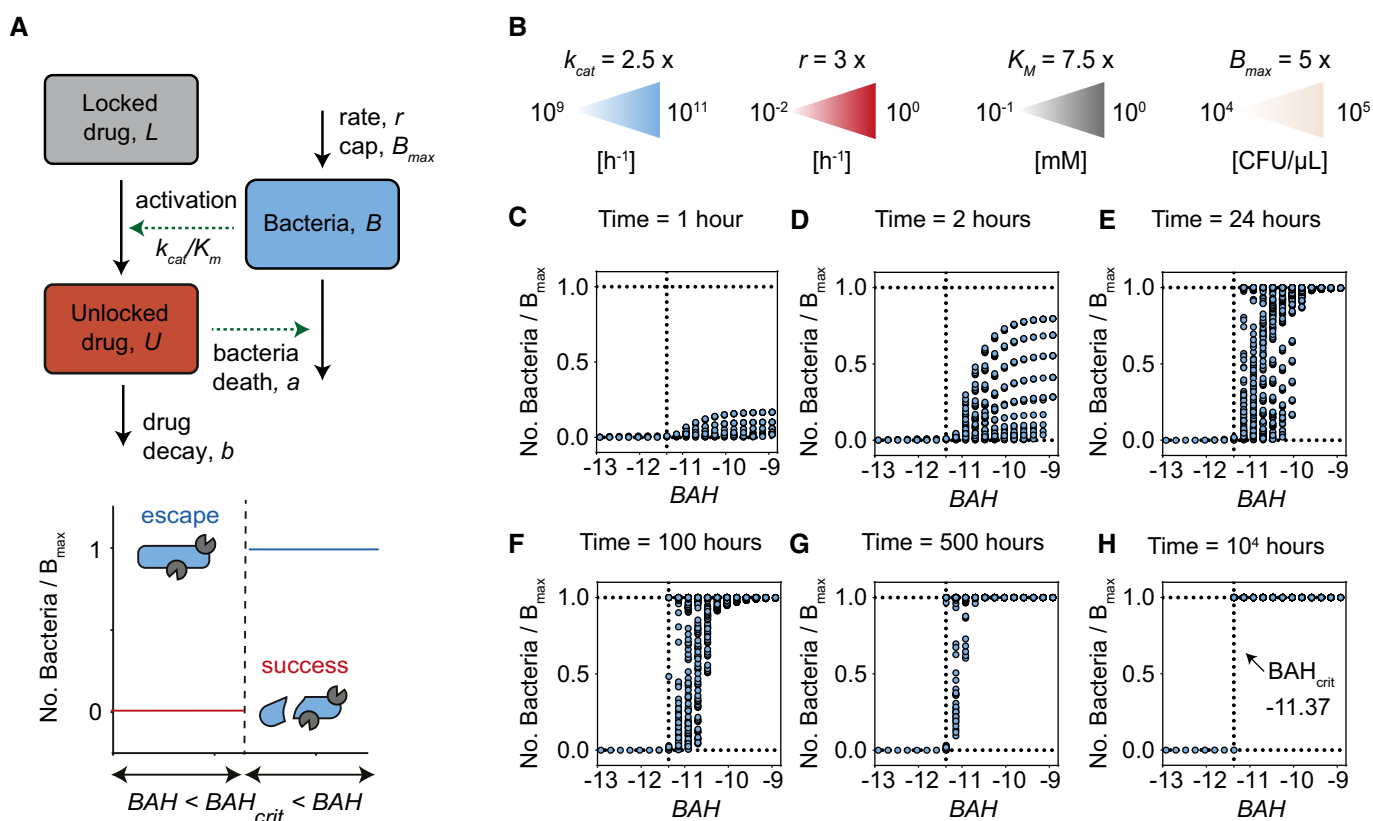
Figure 2. Predicting prodrug success with a dimensionless parameter.

A   (Top) Schematic of general mass action model of bacteria-activated prodrug therapies. Each arrow represents a biological process and is labeled with the system parameters related to that process. Solid black arrows represent growth or decay expressions, and green arrows represent when one population influences the growth or decay expression of another population (e.g., bacteria activate locked drug population). (Bottom) Schematic plot of predicted relationship between *BAH* value and final number of living bacteria (normalized by B_{max}). Conditions where bacteria numbers reach carrying capacity (blue line) are called prodrug escape conditions. Conditions where bacteria numbers reach 0 (red line) are called prodrug success conditions. The vertical dashed line represents the critical *BAH* value (i.e., BAH_{crit}), the point at which the condition switches from prodrug success to prodrug escape. Blue ovals with gray pac mans represent bacteria either surviving (whole), or dying (fragmented).

B   Legend showing the range of parameters used in the computational simulations. The range of each parameter is calculated by multiplying a constant base value (top number) with logarithmically spaced values between two powers of 10 (left and right values). The units are displayed below in brackets.

C–H   Scatter plots showing the number of bacteria surviving (No. Bacteria) at a particular time point (time point in graph title), normalized by the carrying capacity (B_{max}) (y-axis), versus the *BAH* value for that system (x-axis). Horizontal dashed lines represent upper and lower limits to bacteria number (i.e., 0 = all bacteria dead, 1 = bacteria reached carrying capacity). Vertical dashed line represents computationally derived critical *BAH* value (i.e., BAH_{crit}) at which systems switch prodrug success (0) to prodrug escape (1).

revealing a critical value of *BAH* ($BAH_{crit} \sim -11.37$) (Fig 2F–H). In other words, the model predicts that for any environmental condition that produces a $BAH > BAH_{crit}$, the bacteria will ultimately escape the prodrug treatment, and for $BAH < BAH_{crit}$, the bacteria will die (i.e., prodrug success). These dimensionless parameters may be important for guiding the successful design and administration of prodrug therapies, which can be improved by optimizing fundamental pharmacokinetic parameters.

A bacteria-activatable AMP prodrug targets *E. coli* protease OmpT

To validate the predictions of our mathematical model with an *in vitro* bacteria-activated prodrug system, we synthesized a protease-activated AMP prodrug. This AMP prodrug comprised cationic (polyarginine, R_9) antimicrobial peptides (AMP) in charge complexation with anionic peptide locks (polyglutamic acid, E_{13}) by a linker peptide (RRS|RRV) specific for the ubiquitous bacterial protease OmpT (Olson *et al*, 2009; preprint: Holt *et al*, 2019). Upon proteolytic cleavage of the linker, the hairpin prodrug is unlocked to release free AMP (Fig 3A). To measure OmpT activity, we synthesized an activity probe (McCarter *et al*, 2004; Kwong *et al*, 2013, 2021; Holt *et al*, 2017, 2018; Mac *et al*, 2019; Zhuang *et al*, 2019) with free linker peptides containing a fluorophore-quencher pair, which produced an increase in fluorescence upon proteolytic cleavage. To demonstrate linker specificity for OmpT, we incubated the activity probe with OmpT genetic knockout bacteria, as well as the parent background strain (*E. coli* K-12 BW25113), and only observed activity in samples incubated with the parent strain (i.e., OmpT-positive) (Fig 3B). We also observed no activity in samples containing the serine protease inhibitor, Aprotinin, which inhibits OmpT when present in micromolar concentrations (Brannon *et al*, 2015), confirming the linker specificity for OmpT (Fig 3C). We observed a similar cleavage activity using this linker substrate when fully integrated into hairpin AMP drug-lock complexes, confirming that linker presentation within a constrained conformational state did not significantly affect cleavage activity by OmpT (Fig 3D). To measure the cytotoxicity of the unlocked drug, we dosed bacteria with free AMP and observed significant reduction in colonies compared to untreated controls (blue bars) (Fig 3E and F). To confirm prodrug specificity, we synthesized AMP drug-lock complexes using linker peptides specific for OmpT or tobacco etch virus (TEV) protease, which exhibits orthogonal protease specificity (Kapust *et al*, 2001). We observed elimination of bacteria only in samples containing OmpT-specific AMP prodrug (gray bars) or samples treated with both TEV and TEV-specific AMP prodrug (red bars). All control samples containing either TEV-specific prodrug alone or Aprotinin inhibitor did not significantly reduce bacteria load (Fig 3E and F, Table EV1). These results showed that AMP drug-lock complexes are inert and lack cytotoxic activity until activation by protease activity.

Validating the model and predicting prodrug success with an AMP Prodrug and DH5α *E. coli*

We sought to fit our computational model to this experimental bacteria-prodrug system (AMP prodrug + DH5α *E. coli*) (Fig 4A) and demonstrate that the dimensionless parameter *BAH* can predict which conditions are favorable to prodrug success. Rather than using global parameter fitting method after the final system was tested (i.e., bacteria + prodrugs), we individually measured the values for each of the relevant parameters experimentally, including enzymatic efficiency (e.g., k_{cat}, K_M), bacterial growth (e.g., r, B_{max}), and prodrug activity (e.g., a, b) in isolated systems (e.g., bacteria alone, enzymes alone, bacteria + activity-probe, etc.) (Figs EV1–EV3, Tables EV2 and EV3). This allowed us to more rigorously test the model by predicting bacteria-prodrug response curves across nine distinct combinations of k_{cat} and r values before performing the physical experiments. We experimentally controlled the nine distinct combinations of k_{cat} and r values by altering the ambient temperature and concentration of broth (conditions labeled A1–3, B1–3, and C1–3; Table EV3). We affected the enzymatic activation rate of the prodrug, k_{cat}, by changing temperature as described by the Arrhenius equation (Calvert, 1990). Our model anticipated two possible steady-state outcomes to prodrug treatment; bacteria were predicted to be either susceptible to the prodrug and die or to escape prodrug treatment and proliferate to saturating levels (Fig 3). To experimentally validate this, we incubated bacteria with AMP prodrug under the defined nine conditions and quantified the number of living bacteria longitudinally over the course of a 24-h treatment window. Quantified bacterial counts taken during treatment closely matched the values predicted by our model (red and blue dots; Figs 4B and C, and EV4). Furthermore, our model predicted that the dimensionless parameter, *BAH*, would separate prodrug success conditions from prodrug failure conditions. We calculated the *BAH* values for each of the nine conditions (Table EV3) and plotted against the final bacteria number (normalized by B_{max}), which revealed that a critical *BAH* (BAH_{crit}) clearly predicted the conditions where prodrug treatment was favorable (Fig 4D). By receiver-operating-characteristic (ROC) analysis, BAH_{crit} perfectly predicted the conditions where prodrug treatment succeeded (AUROC = 1.00, $n = 9$) with 100% specificity and sensitivity. By comparison, the unlocked drug control (i.e., free polyarginine) successfully treated bacteria in all nine conditions tested (Fig EV4). We next sought to demonstrate an experimental example of how the BAH_{crit} could be used to guide successful prodrug treatment. Our model results predicted that changing key system parameters to decrease the *BAH* below the critical threshold will result in successful treatment of bacteria. To demonstrate this, we took three different AMP prodrugs with distinct linker sequences (Table EV1), which served to increase k_{cat} values for OmpT, thereby decreasing the *BAH* value below BAH_{crit}. By treating the same population of bacteria with a prodrug that has a slightly faster activation rate, we were able to successfully treat bacteria which previously escaped prodrug treatment (Fig EV5). Collectively, these experiments demonstrate that when *E. coli* are exposed to the AMP prodrug, our model can be used to predict bacterial growth kinetics that closely match experimental observation. Furthermore, the *BAH* is a robust predictor of high-level outcomes (i.e., success or failure) across the treatment conditions tested.

Validating the model and predicting prodrug success with TM-TMP and UTI89 *E. coli*

We next sought to validate our model with an orthogonal bacteria-prodrug pair, for which we used the strain UTI89 *E. coli*, which has
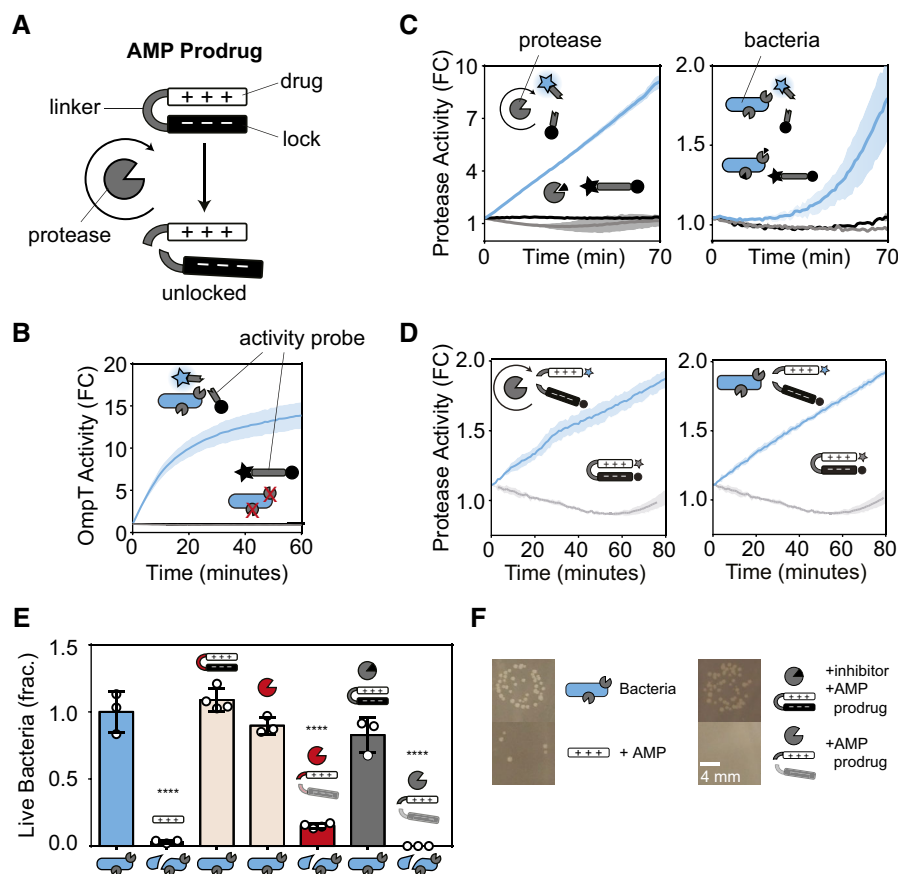
Figure 3. A bacteria-activatable prodrug targets *E. coli* protease OmpT.

A   A cationic AMP drug (R_9, white rectangle) locked by an anionic peptide lock (E_{13}, black rectangle) with a protease-cleavable linker (RRSIRRV, gray u-shape) is activated by OmpT protease (gray pac man) activity.

B   Cleavage assay measuring the activity of OmpT expressed on the surface of parent strain *E. coli* K-12 BW25113 (OmpT-positive; blue bacteria with gray pac mans, top) as well as OmpT genetic knockouts (OmpT-negative; blue bacteria with red X's). Activity is measured using an activity probe, comprising a linear peptide substrate (gray bar) with a fluorophore (blue/gray star) and quencher (black circle) on either end.

C   Cleavage assay using activity probes to measure the activity of recombinant OmpT (gray protease) (left) and OmpT expressed on the surface of *E. coli* bacteria (right), plotted as the blue lines on the graph. Negative control samples contain the inhibitor aprotinin (black triangle) or linker substrates alone (i.e., no proteases added), which are plotted as black and gray lines, respectively.

D   Cleavage assay measuring the activity of recombinant OmpT (left) or OmpT expressed on the surface of *E. coli* (right) against fluorescently labeled hairpin prodrugs (blue lines) or hairpin prodrugs only control (gray lines).

E   Bacteria viability assay quantifying drug toxicity relative to untreated bacteria control (blue bar). Positive control for AMP toxicity (black bar). Negative control for locked AMP or TEV protease alone (tan bars). Positive control for TEV protease (red pac man) with locked AMP (substrate: ENLYFQIG, specific to TEV protease) (red bar). Negative control for locked AMP (substrate: RRSRRV, specific to OmpT) with OmpT inhibitor, aprotinin (gray bar). Experimental condition of bacteria treated with locked AMP activated by natively expressed OmpT (far right bar). All values normalized and compared to bacteria only control via one-way ANOVA, and are plotted as fraction of bacteria only control (y-axis, fraction). Error bars represent standard deviation ($n = 3$–4 biological replicates). ****$P < 0.0001$.

F   Representative images of bacterial plates used to quantify viability with schematic legend (scale bar = 4 mm).

Data information: For all line graphs, shaded regions represent standard deviation ($n = 3$ biological replicates). All cleavage assays (i.e., line graphs) plotted as fold change (FC) in relative fluorescence units (RFU) from initial time point.

---

been used in mouse models of urinary tract infections (Mysorekar & Hultgren, 2006; Hung *et al*, 2009), in combination with a thiomaltose (TM)-conjugated prodrug of the common antibiotic trimethoprim (TMP) (Forsch *et al*, 2004; Ho & Juurlink, 2011), known as TM-TMP (Wang *et al*, 2018). Conjugating thiomaltose to trimethoprim has been shown to increase the water solubility of TMP by 100-fold, while being stable to serum enzymes and maintaining activity against urinary tract infections in mice (Wang *et al*, 2018). In this formulation, thiomaltose serves as a targeting ligand by

complexing the prodrug with maltodextrin transporters, which are exclusively expressed by bacteria, relative to mammalian cells (Fig 5A, step 1) (Wang *et al*, 2018). Then, thiomaltose is conjugated to TMP via a self-immolative disulfide linker that releases TMP-OH, which is as active as TMP, upon disulfide cleavage by free thiols (Fig 5A, step 2; Fig EV6), resulting in the killing of bacteria (Fig 5A, step 3). When comparing the relative bacterial toxicity of TMP (parent drug) and TM-TMP (prodrug) under one set of environmental conditions (i.e., 37°C, 75% broth), we found that the parent drug
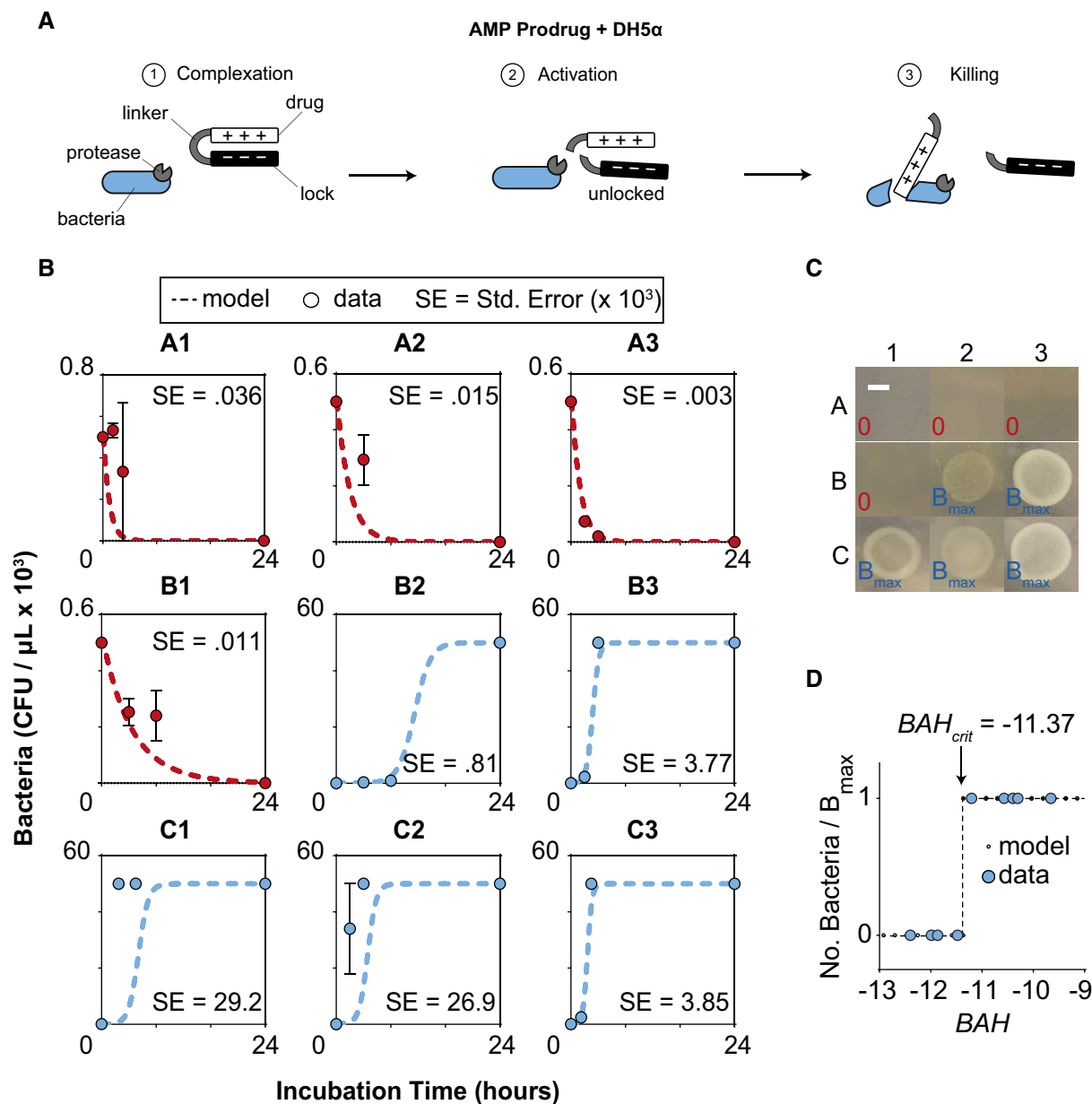
Figure 4. Validating the model and predicting prodrug success with *E. coli* DH5a and AMP Prodrug.

A Graphical representation of the activation of an AMP prodrug (black and white U-shape) by a membrane protease (gray pac man, OmpT) on a bacteria (blue). The AMP prodrug first (step 1) complexes with a membrane-bound protease. The protease enzymatically cleaves the AMP prodrug, thereby, activating the prodrug (step 2). The freed AMP kills the bacteria by intercalating with the membrane causing fatal damage (step 3).

B Validating the model with serial CFU measurements (red and blue dots; $n = 3$ biological replicates, error bars SEM) and ODE model simulations of nine conditions (A1–3, B1–3, C1–3) given extracted growth rate and enzyme kinetics parameter values. Standard error (SE) represents the difference between model predictions and experimental observation.

C Agar plates taken at endpoint plotting the resulting bacterial growth for nine environmental conditions (A1–C3, scale bar = 4 mm).

D Plotting the resulting endpoint bacterial growth for each of the nine conditions (plotted as number of bacteria normalized by carrying capacity B_{max}) versus the calculated *BAH* number (blue dots). This is compared against the values predicted by the model (black dots). The critical *BAH* value that separates prodrug success conditions from prodrug failure conditions is represented by the vertical dashed line (i.e., $BAH_{crit} = -11.37$).

was significantly more efficient at killing UTI89 bacteria (Fig 5B; minimum inhibitory concentration (MIC), $MIC_{TMP} = 3.2$ µM versus $MIC_{TM-TMP} = 50$ µM; $n = 3$), which closely matched results from a separate study (Wang *et al*, 2018). We hypothesized that the

prodrug was less effective because the BAH value in this experiment was above the critical threshold, indicating conditions favorable to prodrug escape. To test this, we calculated the BAH for this experiment (Fig 5B, $BAH = -10.7$) and found that it was indeed higher

than the critical threshold (Fig EV7, $BAH_{crit} = -11.3$), suggesting that prodrug would succeed if the bacterial growth rate was decreased by at least an order of magnitude. To verify this

experimentally, we examined the same conditions (e.g., TMP versus TM-TMP) at one drug concentration (10 μM), but decreased the broth concentration to significantly reduce the bacterial growth rate,
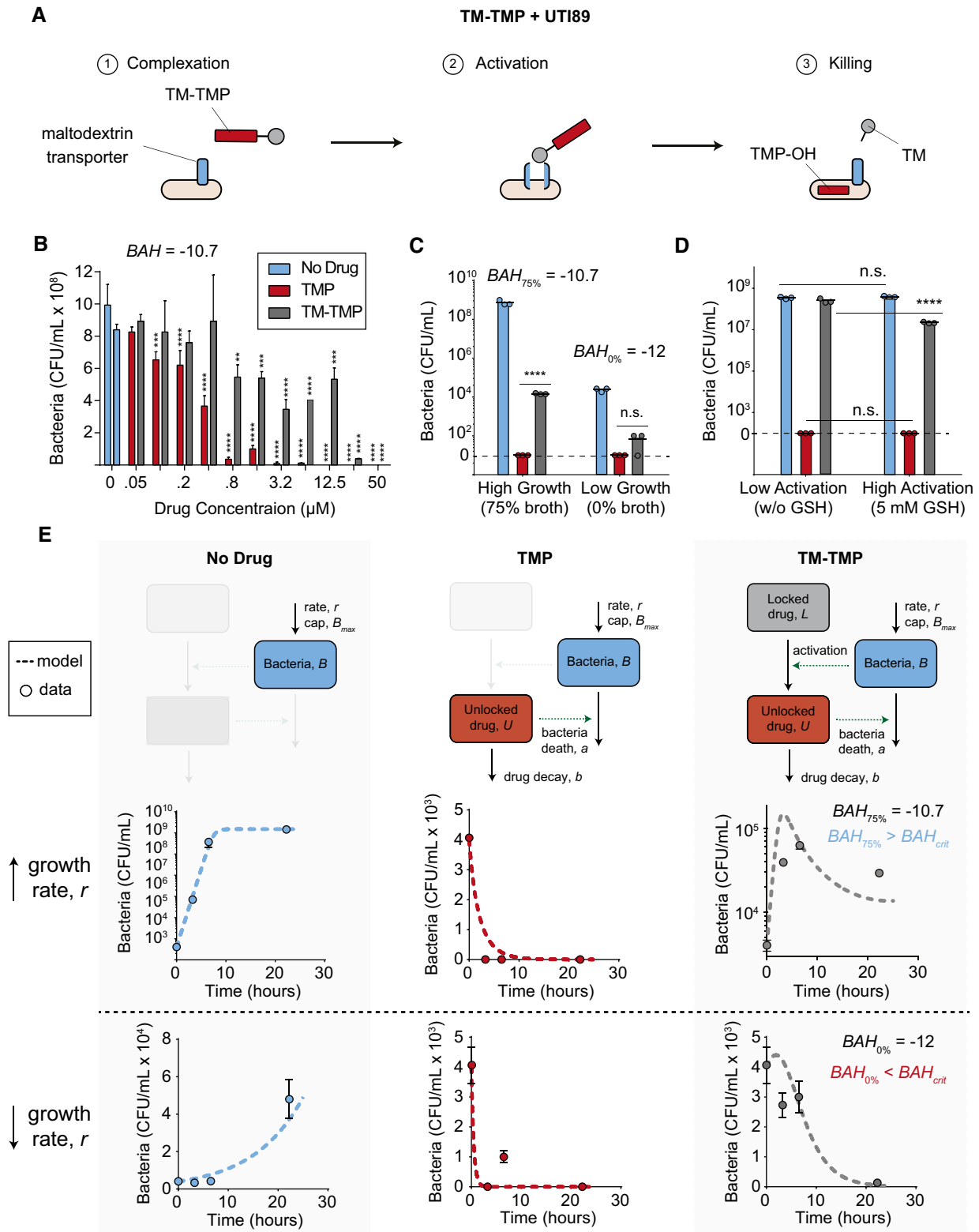

Figure 5.

Figure 5. Validating the model and predicting prodrug success with TM-TMP and UTI89 *E. coli*.

A Schematic of the activation mechanism for the prodrug TM-TMP with the bacteria UTI89 *E. coli*. The thiomaltose (TM, gray) subcomponent first complexes with maltodextrin transporters (blue) on the surface of bacteria (tan) (step 1). The disulfide self-immolative linkage connecting TM to trimethoprim (TMP, red) is cleaved by thiols, releasing free TMP-OH and thus activating the drug (step 2). Free TMP-OH kills the bacteria (step 3).

B Measuring the toxicity of free TMP (red) and prodrug TM-TMP (gray) against UTI89, when compared to no treatment (blue). A range of drug concentrations are incubated with bacteria and the final concentration of living bacteria is measured (*n* = 3 biological replicates; bar height = mean, error bars = standard deviation; one-way ANOVA + Dunnett's multiple comparisons test).

C Measuring the number of surviving bacteria under different growth conditions (i.e., high, 75%, or low, 0%, broth concentration). Bacteria plus no drug (blue), free drug (i.e., TMP, red) and prodrug (i.e., TM-TMP, gray) are incubated in 0% broth (i.e., PBS) or 75% broth (*n* = 3 biological replicates; bar height = mean, error bars = standard deviation; one-way ANOVA + Tukey's multiple comparisons test).

D Measuring the number of surviving bacteria under different drug activation rates (i.e., the presence or absence of glutathione, GSH). Bacteria plus no drug (blue), free drug (i.e., TMP, red) and prodrug (i.e., TM-TMP, gray) are incubated with no GSH, or 5 mM GSH, which increases the activation rate of the prodrug.

E Plotting longitudinal measurements of living bacteria over time under different drug treatment conditions. Each column represents the drug treatment (no drug = blue, TMP = red, and TM-TMP = gray), as labeled in the title. Each row represents the environmental condition affecting growth rate (top row, low growth rate = 0% broth; bottom row, high growth rate = 75% broth). Each plot shows the concentration of bacteria (CFU/ml) over time. Circles with error bars (standard deviation) are experimental measurements (*n* = 3 biological replicates) and dashed lines are predicted by the computational model.

Data information: All conditions in (c) and (d) are compared using one-way ANOVA with multiple comparisons test. All comparisons are made in reference to the bacteria only control (blue bars) **$P < 0.01$, ***$P < 0.001$, and ****$P < 0.0001$.

---

r, (i.e., approximately 1.23 orders of magnitude; $r_{75\%} = 1.7$ s^{-1} versus $r_{0\%} = 0.1$ s^{-1}) which decreased the *BAH* value. We observed that by decreasing the *BAH* value below BAH_{crit} (i.e., $BAH_{75\%} = -10.8$ versus $BAH_{0\%} = -12$), the efficacy of the prodrug was significantly increased and the parent drug (TMP) and the prodrug (TM-TMP) performed more similarly (Fig 5C). To verify this with a second experiment, we also decreased the *BAH* via changing the activation rate of the prodrug, k_{cat}, by spiking in glutathione (GSH), which rapidly hydrolyzes TM-TMP (Wang *et al*, 2018). We found that by adding in GSH (5 mM GSH condition), the number of bacteria killed by TM-TMP (prodrug) was significantly increased, whereas the bacterial counts did not significantly change in either the TMP (parent drug) condition or negative control (no drug) (Fig 5D). These results demonstrated that using the *BAH* as a guiding parameter enabled us to predict the conditions most conducive to prodrug success. Next, we sought to determine whether the computational model associated with the *BAH* (Fig 1) closely matched the kinetics of bacterial growth with this new bacteria-prodrug pair. To validate the model, we started by testing the bacteria population only (negative control) and then built up to the full model by adding in the unlocked drug and the locked drug populations in a stepwise manner (i.e., (i) no drug, (ii) TMP = unlocked drug, and (iii) TM-TMP = locked drug) (Fig 5E, top row). For each version of the model (i.e., each column), we tested both a high bacterial growth rate, *r*, (Fig 5E, middle row) and a low bacterial growth rate (Fig 5E, bottom row), which we controlled by changing the broth concentration. First, by measuring the kinetics of the bacteria population alone, we were able to measure key system parameters (e.g., bacterial growth rate, *r*, and bacterial carrying capacity, B_{max}), which resulted in a close match between experimental and computational results (Fig 5E, left column). Just as with our earlier experiments, we measured (i) the number of bacteria and (ii) the number of drug molecules consumed in each killing reaction to calculate the parameters *a* and *b*, respectively (Fig EV8). Using these parameter values, we used the computational model to predict bacteria population kinetics at high and low growth rates when dosed with TMP (parent drug), which closely matched our experimental results (Fig 5E, middle column). Finally, both the model and the *BAH* value correctly predicted whether the TM-TMP (prodrug) would successfully treat bacteria (i.e., population decays over time) or whether the bacteria would escape treatment (i.e., population grows over time; Fig 5E, right column). These results confirm that our model matches experimental kinetics and that the *BAH* parameter can be used to predict conditions that favor prodrug success.

Discussion

The advantages of prodrugs (e.g., increased solubility, pathogen targeting, etc.) are becoming more widely recognized in contemporary drug design (Rautio *et al*, 2018b). While there have been many studies on bacterial resistance strategies that affect traditional antibiotics (i.e., parent drug), comparatively little attention has been given to studying success/failure conditions specific to prodrugs. To study success and failure conditions in prodrugs, we developed a mathematical model of the competition between bacterial growth and prodrug activation rates. We found that our general model fit the experimental observations from both *in vitro* prodrug-bacteria systems well, while only modifying parameter values between systems. However, future work may improve the model by testing systems with distinct structures such as multistep activation mechanisms, multiple bacterial phenotypes, or dynamic parameter values. While this work held parameters *a* and *b* constant within each system (Tables EV2 and EV4), the model predictions could be further improved by measuring these constants under all environmental conditions. Furthermore, subsequent iterations may also incorporate different models for drug killing (e.g., E_{max}) (Holford, 2017) or bacterial growth (de Jong *et al*, 2017).

From our model, we derived a dimensionless parameter, *BAH*, that predicted the transition between prodrug escape and successful treatment. We found that these prodrugs failed in conditions where bacterial growth outpaced the rate of prodrug activation, as predicted by our computational results. This feedback (i.e., feedback loop; Fig 1B) between bacterial density and drug concentration is similar to the feedback between bacterial density and antibiotics in the inoculum effect (Tan *et al*, 2012), or the feedback between drug-insensitive cells and drug-sensitive cells in multidrug adaptive therapies for cancer (West *et al*, 2020). We demonstrated that both

environmental (e.g., temperature, available nutrients) and pharmacokinetic (e.g., activation rate k_{cat}) parameters can be tuned to engineer successful prodrug therapies. These findings may reveal opportunities for improvement in prodrug design; for example, this information could be leveraged to improve the efficacy of existing prodrugs by tuning the rate of prodrug decay (i.e., biological half-life), which influences the BAH_{crit} transition value (Fig EV9). Alternatively, the catalytic efficiency of the prodrug substrate could be tuned to increase the probability of success, which has been previously demonstrated by engineering prodrug substrates with higher affinity for the enzymatic target (Jordan *et al*, 1999; Barak *et al*, 2006). Importantly, the *BAH* provides a quantitative target for such design modifications and is specific to the nature of prodrugs.

By comparison, previous studies which focused solely on bacterial resistance to the parent form of antibiotics yielded parameters that may not apply to prodrug forms. For example, the minimum inhibitory concentration (MIC) is commonly used as a parameter for resistance (Brauner *et al*, 2016), yet the MIC of the parent and proforms of the same drug can differ, as seen with both model prodrugs used in this study as well as others from the literature (Wang *et al*, 2018; Evans *et al*, 2019; Yang *et al*, 2021). Using existing MIC classifications, these prodrugs could have been labeled ineffective; yet, our experiments showed that different environmental conditions or, in the case of AMP prodrugs, linker sequences, may result in success. One possible reason for the discrepancy in MIC in our studies is that there are kinetic parameters (e.g., drug activation rate) which do not apply to the parent drug, but are key driving factors in determining the outcome of prodrug treatment. Future iterations of this work and the *BAH* may result in a standardized quantitative design criteria that is specific to prodrugs. This is supported by the fact that even with nonprodrugs, metrics such as the single-cell MIC (Artemova *et al*, 2015) and others based on bacterial temporal dynamics (Meredith *et al*, 2015) have been developed for predicting treatment outcomes where MIC fails.

Dimensionless parameters like the *BAH* are commonly used in engineering to create metrics that are consistent across unit-systems (e.g., metric versus imperial) and scales (i.e., the relative size of the variables). In the AMP prodrug system, we found that the transition between prodrug escape and successful treatment occurred sharply at one value (i.e., $BAH_{crit} = -11.3$). By comparison, in the TM-TMP system this transition occurred across a range of values (i.e., $-11.5 < BAH_{crit} < -11.1$), which mirrors the example of pipe flow where the transition from laminar to turbulent flow occurs across a range of Reynolds numbers (i.e., $2{,}300 < \text{Re} < 4{,}000$). Interestingly, both the BAH_{crit} values (-11.3 versus -11.5 to -11.1) and the ratios of *a* to *b* (0.5×10^{-11} versus 3×10^{-11}; Tables EV2 and EV4) were similar between systems, which is consistent with our simulations predicting the dependence of the BAH_{crit} value on the ratio *a* to *b* (Fig EV9). Furthermore, dimensionless parameters measured in model systems can be used to make predictions about scaled-up versions of the same system (i.e., similitude). Analogously, future work may show that the *BAH* could be used to predict which prodrugs are most likely to succeed in clinical settings based on smaller scale preliminary studies.

In clinical settings, prodrug failure could potentially be caused by environmental perturbations (e.g., temperature, pH, etc.) as demonstrated in this work, or by genetic mutations that affect pathogen growth rates (Jin *et al*, 2012) or enzymatic activity (Kramer *et al*,

2000, 2001). We predict that mutations affecting the prodrug-activating enzyme (i.e., k_{cat}) are the more likely cause of prodrug failure because these mutations are localized to one protein, rather than a cascade of events as in the case of growth rate (*r*) (Jin *et al*, 2012). Based on protein expression numbers alone (Thomassin *et al*, 2012) the range of effective k_{cat} values is at least one to two orders of magnitude higher on average than the range of potential growth rate values (Allen & Waclaw, 2019; Weissman *et al*, 2021), which means mutations affecting enzyme activity can have a larger impact on the *BAH* value. Furthermore, there are multiple examples of clinical prodrugs with known bacterial resistance mechanisms linked to enzyme mutations. For example, the nitroimidazole class of antibiotics (e.g., metronidazole, dimetridazole, tinidazole, etc.), which is used to treat anaerobic bacteria (e.g., *Enterococcus* species, *Clostridium* species, *Helicobacter pylori*, etc.) represent prodrugs that are activated by bacterial reductases (Edwards, 1993). Genetic studies have revealed that bacterial resistance to nitroimidazole antibiotics is caused by either partial or complete reduction in expression of genes (e.g., rdxA, frxA, etc.) encoding the reductases that activate the prodrug (Jenks *et al*, 1999; Marais *et al*, 2003; Leiros *et al*, 2004). As another example, the major cause of resistance to nitrofuran prodrugs are mutations to *nfsA* and *nfsB*, which are the enzymes responsible for activating the nitrofuran compound (Le & Rakonjac, 2021).

Here, we quantitatively studied the driving parameters that predict the transition between prodrug escape and successful treatment. We envision that this body of work will improve the process of prodrug development by providing a quantitative metric for predicting success, ultimately helping to reduce the burden of antibiotic failure.

Materials and Methods

Protease cleavage assays

All protease cleavage assays were performed with a BioTek Cytation 5 Imaging Plate Reader, taking fluorescent measurements at 485/528 nm (excitation/emission) for read-outs measuring peptide substrates terminated with FITC (Fluorescein isothiocyanate). Kinetic measurements were taken every minute over the course of 60–120 min at 37°C. Tobacco etch virus protease (TEVp), along with its substrate and buffer was obtained from Anaspec, Inc. (Fremont, CA). Activity RFU measurements were normalized to time 0 measurement, and as such represent fold change in signal. Outer Membrane Protease T (i.e., OmpT, Protease 7) was purchased from Lifespan Biosciences (Seattle, WA). OmpT fluorescent peptide substrate was custom ordered from Genscript (Piscataway, NJ).

Bacterial culture and cytotoxicity measurement

DH5α *Escherichia coli* were a gift from Todd Sulchek's BioMEMS lab at Georgia Tech. *E. coli* were cultured in LB broth (Lennox) at 37°C and plated on LB agar (Lennox) plates. LB broth was purchased from Millipore Sigma (Burlington, MA) and LB agar was purchased from Invitrogen (Carlsbad, CA). AMP and locked AMP were custom ordered from Genscript (Piscataway, NJ). See Table EV1 for more information. Bacteria were grown to a concentration of 10^9 CFU/ml

before being used for experiments. Concentration was estimated by measuring the OD_{600} of the bacterial suspension, and assuming an OD_{600} of 1.000 corresponds to a concentration of 8×10^8 CFU/ml. Bacterial cell viability was measured by making eight 10-fold serial dilutions, and plating three 10-μl spots on an LB agar plate. Plates were incubated overnight at 37°C, and CFUs were counted. Untreated bacteria CFU counts served as control for 0% cytotoxicity, and bacteria + IPA (or 0 countable CFUs) served as control for 100% cytotoxicity.

Computational model

The ODE modelling and solutions were performed in MATLAB 2020b. Code can be found in supplementary information.

Statistical analysis

Statistical analysis was performed using statistical packages included in GraphPad Prism 6. To assess the significance of an increase in signal due to protease cleavage, we used a two-way ANOVA (without repeated measures) followed by Sidak's multiple comparisons test. A one-way ANOVA followed by Dunnett's multiple comparisons test was used to compare experimental means to cells only control bacterial viability assays. Two-way ANOVA followed by Sidak's multiple comparisons test used to compare experimental means to control for bacterial cytotoxicity at multiple starting concentrations.

Supplementary analysis

To determine which steady-state solution is the stable steady-state for our model, we perform a linear stability analysis on the system of differential equations.

First, we rewrite the model in dimensionless variables and parameters:

$$\dot{X}/k_{cat} = \pi_1 X(1-X) - \pi_2 XZ$$

$$\dot{Y}/k_{cat} = -\pi_3 X \frac{Y}{1+Y}$$

$$\dot{Z}/k_{cat} = \pi_3 X \frac{Y}{1+Y} - \pi_4 XZ$$

Where the dimensionless variables are defined as:

$$X = \frac{B}{B_{max}}, \quad Y = \frac{L}{K_M}, \quad Z = \frac{U}{K_M}$$

And the dimensionless parameters are defined as:

$$\pi_1 = \frac{r}{k_{cat}}, \quad \pi_2 = \frac{aK_M}{k_{cat}}, \quad \pi_3 = \frac{B_{max}}{K_M}, \quad \pi_4 = \frac{bB_{max}}{k_{cat}}$$

Steady-state Solution 1: For the steady-state solution where $B = 0$, the dimensionless variable solutions that follow are:

$$X = 0, \quad Y = \frac{1}{\frac{\pi_2 \pi_3}{\pi_1 \pi_4} - 1}, \quad Z = \frac{\pi_1}{\pi_2}$$

The resulting Jacobian, J, and eigenvalues, λ, are:

$$J = \begin{bmatrix} 0 & 0 & 0 \\ -\pi_1\pi_4/\pi_2 & 0 & 0 \\ 0 & 0 & 0 \end{bmatrix}, \quad \lambda = 0, \ 0, \ 0$$

Steady-state Solution 2: For the steady-state solution where $B = B_{max}$, the dimensionless variable solutions that follow are:

$$X = 1, \quad Y = 0, \quad Z = 0$$

The resulting Jacobian, J, and eigenvalues, λ, are:

$$J = \begin{bmatrix} -\pi_1 & 0 & 0 \\ 0 & -\pi_3 & 0 \\ 0 & \pi_3 & -\pi_4 \end{bmatrix}, \quad \lambda = -\pi_1, \ -\pi_3, \ -\pi_4$$

Since the eigenvalues for steady-state solution 2 (i.e., $B = B_{max}$) are all negative, whereas the eigenvalues for steady-state solution 1 ($B = 0$) are all equal to 0, we can conclude that steady-state solution 2 is stable and steady-state solution 1 is unstable.

Data availability

The data supporting the findings of this study are available within the paper and EV files. The code is available within the EV files and at https://github.com/brandon-holt/bacterial-advantage-heuristic.

Expanded View for this article is available online.

Author contributions
GAK, NM, and BAH contributed ideas. KGA, BAH, MT, MS, and YX designed experiments and interpreted results. BAH, MT, YX, MS, JJR, and XW carried out experiments. GAK and BAH wrote the manuscript. BAH, MT, YX, MS, NM, and GAK edited the manuscript.

Disclosure statement and competing interests
KGA is co-founder of Glympse Bio, and consults for Glympse Bio and Satellite Bio. This study could affect his personal financial status. The terms of this arrangement have been reviewed and approved by Georgia Tech in accordance with its conflict of interest policies. HBA and KGA are listed as inventors on a

patent application pertaining to the results of the paper. The title of the patent is "Self-titrating, bacterial protease-activated prodrug". The patent applicant is the Georgia Tech Research Corporation and the names of the inventors are Brandon Holt and Gabriel Kwong. The patent is currently pending and the application numbers are 62/733,347 (U.S.) and WO 2020061244A2 (International). The AMP prodrug and the *BAH* are covered in the patent.

References

Al-Badr AA, Ajarim TDS (2018) Chapter one – ganciclovir. In *Profiles of drug substances, excipients and related Methodology*, Brittain HG (ed.), pp 1–208. Cambridge, MA: Academic Press

Allen RJ, Waclaw B (2019) Bacterial growth: a statistical physicist's guide. *Rep Prog Phys* 82: 16601

Artemova T, Gerardin Y, Dudley C, Vega NM, Gore J (2015) Isolated cell behavior drives the evolution of antibiotic resistance. *Mol Syst Biol* 11: 822

Atuegwu NC, Arlinghaus LR, Li X, Chakravarthy AB, Abramson VG, Sanders ME, Yankeelov TE (2013) Parameterizing the logistic model of tumor growth by DW-MRI and DCE-MRI data to predict treatment response and changes in breast cancer cellularity during neoadjuvant chemotherapy. *Translational Oncology* 6: 256–264

Baquero F, Martinez JL, Canton R (2008) Antibiotics and antibiotic resistance in water environments. *Curr Opin Biotechnol* 19: 260–265

Barak Y, Thorne SH, Ackerley DF, Lynch SV, Contag CH, Matin A (2006) New enzyme for reductive cancer chemotherapy, YieF, and its improvement by directed evolution. *Mol Cancer Ther* 5: 97–103

Batchelor GK (2000) *An introduction to fluid dynamics*. Cambridge: Cambridge University Press

Brannon JR, Burk DL, Leclerc J-M, Thomassin J-L, Portt A, Berghuis AM, Gruenheid S, Le Moual H (2015) Inhibition of outer membrane proteases of the omptin family by aprotinin. *Infect Immun* 83: 2300–2311

Brauner A, Fridman O, Gefen O, Balaban NQ (2016) Distinguishing between resistance, tolerance and persistence to antibiotic treatment. *Nat Rev Microbiol* 14: 320

Calvert JG (1990) Glossary of atmospheric chemistry terms (Recommendations 1990). *Pure Appl Chem* 62: 2167–2219

Cho S, Yoon Y-R (2018) Understanding the pharmacokinetics of prodrug and metabolite. *Transl Clin Pharmacol* 26: 1–5

Edwards DI (1993) Nitroimidazole drugs-action and resistance mechanisms I. Mechanism of action. *J Antimicrob Chemother* 31: 9–20

Evans LE, Krishna A, Ma Y, Webb TE, Marshall DC, Tooke CL, Spencer J, Clarke TB, Armstrong A, Edwards AM (2019) Exploitation of antibiotic resistance as a novel drug target: development of a β-lactamase-activated antibacterial prodrug. *J Med Chem* 62: 4411–4425

Forde E, Humphreys H, Greene CM, Fitzgerald-Hughes D, Devocelle M (2014) Potential of host defense peptide prodrugs as neutrophil elastase-dependent anti-infective agents for cystic fibrosis. *Antimicrob Agents Chemother* 58: 978–985

Forsch RA, Queener SF, Rosowsky A (2004) Preliminary *in vitro* studies on two potent, water-soluble trimethoprim analogues with exceptional species selectivity against dihydrofolate reductase from *Pneumocystis carinii* and *Mycobacterium avium*. *Bioorg Med Chem Lett* 14: 1811–1815

Fujikawa H, Kai A, Morozumi S (2003) A new logistic model for bacterial growth. *J Food Hyg Soc Jpn* 44: 155–160

Gullberg E, Cao S, Berg OG, Ilbäck C, Sandegren L, Hughes D, Andersson DI (2011) Selection of resistant bacteria at very low antibiotic concentrations. *PLoS Pathog* 7: e1002158

Ho JM, Juurlink DN (2011) Considerations when prescribing trimethoprim-sulfamethoxazole. *Can Med Assoc J* 183: 1851–1858

Holford N (2017) Pharmacodynamic principles and the time course of immediate drug effects. *Transl Clin Pharmacol* 25: 157–161

Holt BA, Bellavia MC, Potter D, White D, Stowell SR, Sulchek T (2017) Fc microparticles can modulate the physical extent and magnitude of complement activity. *Biomater Sci* 5: 463–474

Holt BA, Curro I, Kwong GA (2019) Prodrug defiance reveals logic-based strategies for treating bacterial resistance. *bioRxiv* https://doi.org/10.1101/556951 [PREPRINT]

Holt BA, Mac QD, Kwong GA (2018) Nanosensors to detect protease activity *in vivo* for noninvasive diagnostics. *J Vis Exp* (137): e57937 https://doi.org/10.3791/57937

Howse GL, Bovill RA, Stephens PJ, Osborn HMI (2019) Synthesis and antibacterial profiles of targeted triclosan derivatives. *Eur J Med Chem* 162: 51–58

Hung C-S, Dodson KW, Hultgren SJ (2009) A murine model of urinary tract infection. *Nat Protoc* 4: 1230–1243

Iizumi T, Battaglia T, Ruiz V, Perez GI (2017) Gut microbiome and antibiotics. *Arch Med Res* 48: 727–734

Jackson TL, Senter PD, Murray JD (2000) Development and validation of a mathematical model to describe anti-cancer prodrug activation by antibody-enzyme conjugates. *J Theoret Med* 2: 389534

Jain M, Sharma GC, Singh A (2009) A theoretical approach for activation of a pro-drug by its conjugate and its localization in cancer chemotherapy. *Mathemat Comput Model* 50: 333–343

Jenks PJ, Ferrero RL, Labigne A (1999) The role of the rdxA gene in the evolution of metronidazole resistance in *Helicobacter pylori*. *J Antimicrob Chemother* 43: 753–758

Jin DJ, Cagliero C, Zhou YN (2012) Growth rate regulation in *Escherichia coli*. *FEMS Microbiol Rev* 36: 269–287

de Jong H, Casagranda S, Giordano N, Cinquemani E, Ropers D, Geiselmann J, Gouzé J-L (2017) Mathematical modelling of microbes: metabolism, gene expression and growth. *J R Soc Interface* 14: 20170502

Jordan AM, Khan TH, Osborn HM, Photiou A, Riley PA (1999) Melanocyte-directed enzyme prodrug therapy (MDEPT): development of a targeted treatment for malignant melanoma. *Bioorg Med Chem* 7: 1775–1780

Jubeh B, Breijyeh Z, Karaman R (2020) Antibacterial prodrugs to overcome bacterial resistance. *Molecules* 25: 1543

Kapust RB, Tözsér J, Fox JD, Anderson DE, Cherry S, Copeland TD, Waugh DS (2001) Tobacco etch virus protease: mechanism of autolysis and rational design of stable mutants with wild-type catalytic proficiency. *Protein Eng Des Sel* 14: 993–1000

Kramer RA, Vandeputte-Rutten L, de Roon GJ, Gros P, Dekker N, Egmond MR (2001) Identification of essential acidic residues of outer membrane protease OmpT supports a novel active site. *FEBS Lett* 505: 426–430

Kramer RA, Zandwijken D, Egmond MR, Dekker N (2000) *In vitro* folding, purification and characterization of *Escherichia coli* outer membrane protease ompT. *Eur J Biochem* 267: 885–893

Kwong GA, Ghosh S, Gamboa L, Patriotis C, Srivastava S, Bhatia SN (2021) Synthetic biomarkers: a twenty-first century path to early cancer detection. *Nat Rev Cancer* 21: 655–668

Kwong GA, von Maltzahn G, Murugappan G, Abudayyeh O, Mo S, Papayannopoulos IA, Sverdlov DY, Liu SB, Warren AD, Popov Y *et al* (2013) Mass-encoded synthetic biomarkers for multiplexed urinary monitoring of disease. *Nat Biotech* 31: 63–70

Le VVH, Rakonjac J (2021) Nitrofurans: revival of an "old" drug class in the fight against antibiotic resistance. *PLoS Pathog* 17: e1009663

Leiros HK, Kozielski-Stuhrmann S, Kapp U, Terradot L, Leonard GA, McSweeney SM (2004) Structural basis of 5-nitroimidazole antibiotic resistance: the crystal structure of NimA from *Deinococcus radiodurans*. *J Biol Chem* 279: 55840–55849

Mac QD, Mathews DV, Kahla JA, Stoffers CM, Delmas OM, Holt BA, Adams AB, Kwong GA (2019) Non-invasive early detection of acute transplant rejection via nanosensors of granzyme B activity. *Nat Biomed Eng* 3: 281–291

Marais A, Bilardi C, Cantet F, Mendz GL, Mégraud F (2003) Characterization of the genes rdxA and frxA involved in metronidazole resistance in *Helicobacter pylori*. *Res Microbiol* 154: 137–144

Marinelli L, Fornasari E, Eusepi P, Ciulla M, Genovese S, Epifano F, Fiorito S, Turkez H, Örtücü S, Mingoia M *et al* (2019) Carvacrol prodrugs as novel antimicrobial agents. *Eur J Med Chem* 178: 515–529

Masters PA, O'Bryan TA, Zurlo J, Miller DQ, Joshi N (2003) Trimethoprim-sulfamethoxazole revisited. *Arch Intern Med* 163: 402–410

McCarter JD, Stephens D, Shoemaker K, Rosenberg S, Kirsch JF, Georgiou G (2004) Substrate specificity of the *Escherichia coli* outer membrane protease OmpT. *J Bacteriol* 186: 5919–5925

Menten L, Michaelis M (1913) Die kinetik der invertinwirkung. *Biochem Z* 49: 333–369

Meredith HR, Lopatkin AJ, Anderson DJ, You L (2015) Bacterial temporal dynamics enable optimal design of antibiotic treatment. *PLoS Comput Biol* 11: e1004201

Metcalfe C, Macdonald IK, Murphy EJ, Brown KA, Raven EL, Moody PC (2008) The tuberculosis prodrug isoniazid bound to activating peroxidases. *J Biol Chem* 283: 6193–6200

Murphy JT, Walshe R, Devocelle M (2011) A theoretical analysis of the prodrug delivery system for treating antibiotic-resistant bacteria. *IEEE/ACM Trans Comput Biol Bioinform* 8: 650–658

Mysorekar IU, Hultgren SJ (2006) Mechanisms of uropathogenic *Escherichia coli* persistence and eradication from the urinary tract. *Proc Natl Acad Sci USA* 103: 14170–14175

Negrya SD, Jasko MV, Solyev PN, Karpenko IL, Efremenkova OV, Vasilyeva BF, Sumarukova IG, Kochetkov SN, Alexandrova LA (2020) Synthesis of water-soluble prodrugs of 5-modified 2'-deoxyuridines and their antibacterial activity. *J Antibiot* 73: 236–246

Nguyen TT, Guedj J, Chachaty E, de Gunzburg J, Andremont A, Mentré F (2014) Mathematical modeling of bacterial kinetics to predict the impact of antibiotic colonic exposure and treatment duration on the amount of resistant enterobacteria excreted. *PLoS Comput Biol* 10: e1003840

Nielsen EI, Cars O, Friberg LE (2011) Pharmacokinetic/pharmacodynamic (PK/PD) indices of antibiotics predicted by a semimechanistic PKPD model: a step toward model-based dose optimization. *Antimicrob Agents Chemother* 55: 4619–4630

Nielsen EI, Viberg A, Löwdin E, Cars O, Karlsson MO, Sandström M (2007) Semimechanistic pharmacokinetic/pharmacodynamic model for assessment of activity of antibacterial agents from time-kill curve experiments. *Antimicrob Agents Chemother* 51: 128–136

Olson ES, Aguilera TA, Jiang T, Ellies LG, Nguyen QT, Wong E, Gross L, Tsien RY (2009) *In vivo* characterization of activatable cell penetrating peptides for targeting protease activity in cancer. *Integr Biol* 1: 382–393

Olson ES, Jiang T, Aguilera TA, Nguyen QT, Ellies LG, Scadeng M, Tsien RY (2010) Activatable cell penetrating peptides linked to nanoparticles as dual probes for *in vivo* fluorescence and MR imaging of proteases. *Proc Natl Acad Sci USA* 107: 4311–4316

Opatowski L, Mandel J, Varon E, Boëlle P-Y, Temime L, Guillemot D (2010) Antibiotic dose impact on resistance selection in the community: a mathematical model of β-lactams and *Streptococcus pneumoniae* dynamics. *Antimicrob Agents Chemother* 54: 2330–2337

Rautio J, Meanwell NA, Di L, Hageman MJ (2018a) The expanding role of prodrugs in contemporary drug design and development. *Nat Rev Drug Discovery* 17: 559

Rautio J, Meanwell NA, Di L, Hageman MJ (2018b) The expanding role of prodrugs in contemporary drug design and development. *Nat Rev Drug Discovery* 17: 559–587

Tan C, Smith RP, Srimani JK, Riccione KA, Prasada S, Kuehn M, You L (2012) The inoculum effect and band-pass bacterial response to periodic antibiotic treatment. *Mol Syst Biol* 8: 617

Thomassin J-L, Brannon JR, Gibbs BF, Gruenheid S, Le Moual H (2012) OmpT outer membrane proteases of enterohemorrhagic and enteropathogenic *Escherichia coli* contribute differently to the degradation of human LL-37. *Infect Immun* 80: 483–492

Verhulst P-F (1845) Mathematical researches into the law of population growth increase. *Nouveaux Mémoires de l'Académie Royale des Sciences et Belles-Lettres de Bruxelles*

Wang X, Borges CA, Ning X, Rafi M, Zhang J, Park B, Takemiya K, Lo Sterzo C, Taylor WR, Riley L *et al* (2018) A trimethoprim conjugate of thiomaltose has enhanced antibacterial efficacy *in vivo*. *Bioconjug Chem* 29: 1729–1735

Weissman JL, Hou S, Fuhrman JA (2021) Estimating maximal microbial growth rates from cultures, metagenomes, and single cells via codon usage patterns. *Proc Natl Acad Sci USA* 118: e2016810118

West J, You L, Zhang J, Gatenby RA, Brown JS, Newton PK, Anderson ARA (2020) Towards multidrug adaptive therapy. *Can Res* 80: 1578–1589

Yang H, Liu K, Jin S, Huigens Iii RW (2021) Design, synthesis and biological evaluation of a halogenated phenazine-erythromycin conjugate prodrug for antibacterial applications. *Org Biomol Chem* 19: 1483–1487

Zhuang Q, Holt BA, Kwong GA, Qiu P (2019) Deconvolving multiplexed protease signatures with substrate reduction and activity clustering. *PLOS Comput Biol* 15: e1006909